USING COMPUTER TECHNIQUE FOR DEVELOPING METHOD FOR VIBRATION DAMAGE ESTIMATION UNDER COMBINED RANDOM AND DETERMINISTIC LOADING

Michał PTAK*, Jerzy CZMOCHOWSKI*

*Department of Machine Design and Research, Wroclaw University of Technology and Science,
ul. Ignacego Łukasiewicza 7/9, 50-371 Wrocław, Poland

michal.ptak@pwr.edu.pl, jerzy.czmochowski@pwr.edu.pl

received 23 March 2023, revised 23 May 2023, accepted 16 June 2023

Abstract: This paper is focusses on developing a novel method for vibration damage estimation for military helicopters, fighter aircrafts and any other aircraft exposed to combined stochastic and deterministic loading. The first stage of the research focused on frequency domain damage prediction, which is the legacy method proposed by Bishop and developed by Sweitzer, Schlesinger, Woodward, Kerr, Murthy, Datta and, Atkins. The mentioned frequency domain-based method is used in commercial software, e.g., MSC CAE Fatigue. Frequency domain damage prediction is based on superposition of spectral moments and Dirlik method of Rainflow Cycle Counting algorithm in frequency domain. The first phase of the research showed the legacy algorithm based on transfer function developed using FEM (Finite Element Method) method in Abaqus environment and is very conservative. The second stage of the research aims to develop a novel method which allowing for more robust and accurate damage estimation. For this purpose, the Monte Carlo method for retrieving random signal in the time domain from signal in frequency domain was used. To obtain the system transfer function, – the 1 g load harmonic system response was obtained using FEM analysis. It was subsequently scaled linearly by the PSD input curve for random loading and sine wave, or sine sweep function for deterministic loading to calculate the cumulative system response of the linear system. The research allows the development of a novel method to precisely estimate vibration damage using combined time and frequency domains approach, based on effective frequency domain FEM analysis of the linear system. The new proposed method can be also used for precise replication of test conditions via considering signal clipping and frequency resolution used for real testing.

Key words: vibration damage, random vibration, FEM, Monte Carlo method, frequency, time domain Rainflow Cycle Counting algorithms

1. INTRODUCTION

Rainflow Cycle Counting algorithm in frequency domain is commonly used for vibration damage estimation under stochastic loading of linear systems in synergy with FEM analysis. A precursor of Rainflow Cycle Counting algorithm in frequency domain was the study of Bendat and Rice [1–4], whose authors provided a method for use in narrow band signals. The next milestone was the development of the Rainflow Cycle Counting algorithm in the frequency domain made by Dirlik, using Monte Carlo method 5. This approach is now considered one of the most accurate techniques used in commercial software applications [6, 7] for assessment of damage under random loading. Other researchers were Lalanne [8–10] and Steinberg 11, who provided their methods for Rainflow Cycle Counting in the frequency domain. All aforementioned methods have been tested by Halfpenny [12–14], albeit only for evaluation of damage under pure stochastic loading.

The aforementioned methods have been developed for vibration damage estimation for purely stochastic loading. However, these methods have been adopted for more general usage i.e. damage estimation under combined stochastic and deterministic loading in the studies of Bishop, Sweitzer, Schlesinger, Woodward, Kerr, Murthy, Datta and Atkins in their publications [15–24]; and the loading scenario for using this method is e.g. simultaneous deterministic sine sweep and random load – as can be seen in Fig. 1. This combination is required by the US Department of Defence Test Method Standard 27 or other specific requirement specified by military aircraft manufacturers.

The first stage of research introduced in this paper shows that using the abovementioned methods has resulted in highly conservative damage results.

The second stage of research was the development of a novel method for precise damage estimation under combined loads, and this method introduces combined frequency and time domain calculation instead of using only frequency domain for vibration damage estimation in the legacy method. Superposition of the stochastic and deterministic loading approaches has been introduced by NASA 28. The novel method presented in this paper assumes an extension of this approach for analysis of the PSD Response of the system, realising the stochastic and deterministic signals' superposition and damage analysis by use of the Monte Carlo method. The novel method introduced in this paper is much more accurate, as well as offers an opportunity to replicate test parameters e.g., clipping the stochastic signal at a considered sigma level. Additionally, this method allows consideration of the large population of time series to assess the damage distribution for a considered PSD input curve.

In this paper, for combined loads, a simultaneous deterministic linear sine sweep was used (which represents, e.g. shooting with the variable firing gun installed on an aircraft or helicopter),

and stochastic loads were defined with the use of a PSD input curve (Fig. 1), which represents normal operating dynamic loading, e.g. turbulences.

The novel technique introduced in this paper expands research carried out by Dirlik in consideration of frequency resolution, populational studies [27, 28], combination stochastic and deterministic loading, and additionally uses FEM for transfer function estimation.

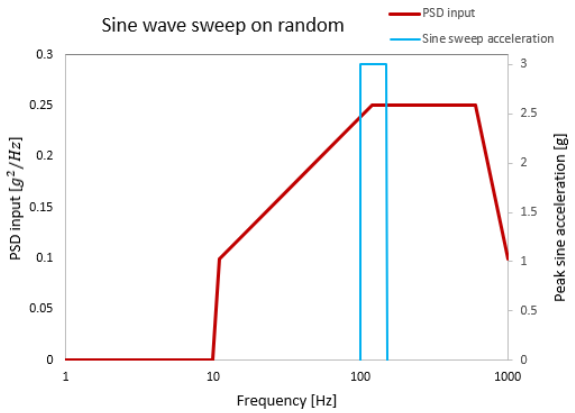

Fig. 1. Sine waves sweep simultaneous with random background

2. FREQUENCY DOMAIN VIBRATION DAMAGE ESTIMATION

Vibration damage assessment, based on transfer function of system, was derived using the mode superposition method in Abaqus environment. The PSD Response functions were founded based on a complex stress tensor (that assumed real and imaginary values), and are used for the evaluation of Huber–Mises–Hencky (σHMH) stress based on Eq. 1:

$$\sigma_{HMH} = \frac{1}{2}[(\sigma_{11} - \sigma_{22})^2 + (\sigma_{22} - \sigma_{33})^2 + (\sigma_{11} - \sigma_{33})^2 + 6(\sigma_{23}^2 + \sigma_{31}^2 + \sigma_{12}^2)] \quad (1)$$

where each stress tensor component is evaluated as shown in Eq. 2:

$$\sigma_{ij} = Re(\sigma_{ij}) + Im(\sigma_{ij}) \quad (2)$$

where $\mathrm{Re}(\sigma_{ij})$ is the real part of stress tensors, and $\mathrm{Im}(\sigma_{ij})$ the imaginary part.

The equivalent stress has been used for demonstration of the algorithm; additionally, this approach is widely used in related publications [12–14, 30, 31], and commercial software applications such as nCode 7 and MSC CAE Fatigue 6, for isotropic material. Future research will focus also on developing algorithms by means of using the Critical Plane approach, which is treated as a more robust approach [6, 7, 30. 31]; however, such an approach would be much more computationally expensive.

It needs to be noted that the original development of this method in the present study is intended for application concerning isotropic, metallic material; any other consideration with reference to usage of this method for orthotropic material will be a subject of future research.

Additionally, the aforementioned further research will focus also on the possibility for using the proposed method in such a way that synergy with the energetic fracture mechanics model is achieved, as can be observed in relevant studies comprised in the literature [32–34], where the Cohesive Zone Model has been used for assessing damage and life prediction.

The derived transfer function H(f) was then multiplied by the PSD input G(f) defined for the considered test duty, and resultantly the PSD Response function in frequency (see Fig. 2) domain was obtained, as indicated in Eq. (3).

$$S(f) = H(f) \cdot G(f) \quad (3)$$

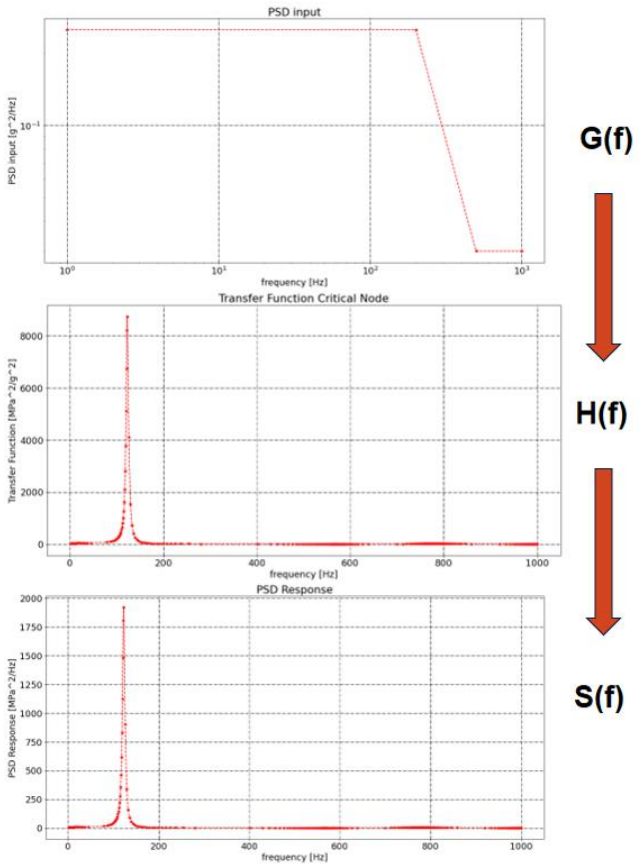

Fig. 2. Evaluation of the PSD Response workflow based on PSD input load and Transfer Function of the considered unit

The PSD Response function has been derived for each integration point of the discrete model. Spectral analysis was the next step to be based on the PSD Response of the considered unit, and it involved numerical integration of the 0th, 1st, 2nd and 4th spectral moments (m_n) in the frequency domain, based on Eq. (4):

$$m_n = \int_0^\infty f^n \cdot S(f) df \quad (4)$$

where $\mathrm{m_n}$ represents the n spectral moment, f the considered frequency and $\mathrm{S(f)}$ the PSD Response function.

Spectral moments are used for derivation of signal statistic parameters in frequency domain:

Upward zero crossing $(\mathrm{E[0]})$ – Eq. (5):

$$E[0] = \sqrt{\frac{m_2}{m_0}} \quad (5)$$

where m_2 stands for the second spectral moment and m_0 the zero spectral moment.

Number of peaks $(\mathrm{E[P]})$ (local maximum of signal function) – Eq. (6):

$$E[P] = \sqrt{\frac{m_4}{m_2}} \tag{6}$$

where m_4 stands for the fourth spectral moment.

Irregular factor (γ) – Eq. (7):

$$\gamma = \frac{m_2}{\sqrt{m_0 \cdot m_4}} \tag{7}$$

Signal statistic parameters in frequency domain constitute the basis for the Dirlik method of executing the Rainflow Cycle Counting algorithm in frequency domain, as can be ascertained from the studies of Dirlik 5 and Bishop et al. 19.

The Probability Density Function (PDF) of Dirlik method (PDFD) can be written in the form indicated by Eq. (8):

$$PDFD = \left(\frac{D_1}{Q} e^{\frac{Z}{Q}} + \frac{D_2 Z}{R^2} e^{\frac{-Z^2}{2R^2}} + D_3 Z e^{\frac{-Z^2}{2}} \right) \cdot \frac{dS}{2RMS} \tag{8}$$

where the normalised Dirlik stress variable is represented by Z (Note: The value of the Dirlik normalised stress variable is twice that of the Bendat normalised stress variable.); as indicated in Eq. (9),

$$Z = \frac{S}{2\sqrt{m_0}} \tag{9}$$

where S is the stress at the considered histogram bin.

The "mean frequency" (X_m) would be as presented in Eq. (10):

$$X_m = \frac{m_1}{m_0} \cdot \sqrt{\frac{m_2}{m_4}} \tag{10}$$

Expressions of the remaining Dirlik empirical variables (D_1, D_2, D_3, Q and R) are presented in Equations (11)–(15):

$$D_1 = \frac{2(X_m - \gamma^2)}{1 + \gamma^2} \tag{11}$$

$$D_2 = \frac{1 - \gamma - D_1 + {D_1}^2}{1 + \gamma^2} \tag{12}$$

$$D_3 = 1 - D_1 - D_2 \tag{13}$$

$$Q = \frac{1.25 \cdot (\gamma - D_2 \cdot R - D_3)}{D_1} \tag{14}$$

$$R = \frac{\gamma - X_m - {D_1}^2}{1 - \gamma - D_1 + {D_1}^2} \tag{15}$$

The final equation for estimation of the actual number of cycles with the use of the Dirlik method (n_{Dirlik}) can be presented as indicated in Eq. (16):

$$n_{Dirlik} = PDFD(S) \cdot T \cdot E[P] \tag{16}$$

where T is the time of exposure on random loading.

Total damage was evaluated using the Palmgren-Miner rule 37 and the failure criterion equivalent to damage value exceeds 1, as indicated in Eq. (17):

$$\text{Total Damage} = \sum_{0}^{\infty} \frac{n_{i\_Dirlik}}{N(S_i)} \tag{17}$$

where n_{i_Dirlik} is the actual number of cycles for the considered stress at bins, and $N(S_i)$ the allowable number of cycles for the considered stress at bins, based on S-N curve (fatigue curve – stress versus available cycles).

As part of the present research, the authors created a tool for damage estimation using an exemplary unit for benchmarking against commercial software. Fatigue damage estimation is based on FEM analysis 39 unit loading with the use of a linear dynamic method in an Abaqus software application 40. This research used the example of a cantilever beam with a cut U notch. The geometry, discrete model and graphical support representation are presented in Fig. 3. The harmonic load input is a unit load (1 g) acceleration applied to the base (supported region).

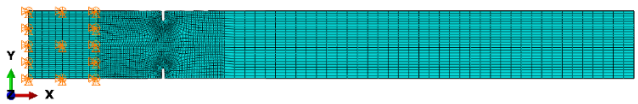

Fig. 3. Geometry, discrete model and graphical support representation of a sample taken for the research results' visualisation

For this paper, it is assumed that the sample is made of steel 17-4PH (H1025), and accordingly, fatigue material properties from MMPDS-15 31 were used; thus, for the considered steel sample, a value of Kt = 3 was used as the reference.

Tab. 1. Steel 17-4PH (H1025) material properties used for demonstrational analysis

Steel 17-4PH (H1025)		
Young modulus E [MPa]	Poisson ratio v [–]	Density ρ [t/mm^3]
195,000	0.27	7.89E–09

To enable an effective consideration of the aforementioned factors, the authors of the present study assumed a constant critical damping ratio for the entirety of the frequency bandwidth (0–1,000 Hz) and equal to 2.5%. (Note that the created method and software need input, which would need to consist of a model correlated against test results; however, for benchmarking, we assumed artificial parameters of damping.)

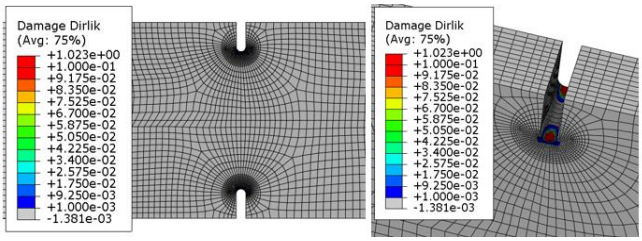

Fig. 4. Frequency domain vibration damage estimation using Dirlik method

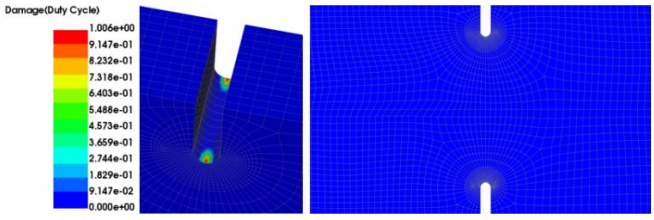

Fig. 5. Visualisation of Dirlik Damage obtained in MSC CAE Fatigue commercial software environment

Damage results can then be presented on a discrete model using Abaqus 40 visualisation module and the authors' scripts, as demonstrated in Fig. 4.

For the considered method, benchmarking has been made against the MSC CAE Fatigue software. An exemplary result for duty matched to the above example is presented in Fig. 5.

The obtained damage values have been benchmarked against commercial software and the differences in results do not exceed 1%. This result is the basis for the first stage of the research – damage estimation for combined stochastic and deterministic loading in frequency domain.

3. FREQUENCY DOMAIN VIBRATION FATIGUE ESTIMATION UNDER COMBINED STOCHASTIC AND DETERMINISTIC LOADING – THE LEGACY METHOD

The methodology introduced in Section 2 of this paper is the basis for damage estimation under only stochastic loading. Research carried out by Bishop, Sweitzer, Schlesinger, Woodward, Kerr, Murthy, Datta and Atkins in their publications [15–24] describe the idea for damage estimation based on superimposition of spectral moments generated by random and deterministic loads. The abovementioned approach was used in these studies.

The transfer function $(\mathrm{Hi(f)})$, which consists of e.g. Huber–Mises–Hencky complex stress or critical plane stress, needs to be evaluated for finite i numbers of frequency sub-ranges, e.g. for a sweep between 100 Hz and 150 Hz, there is a need for the evaluation to be conducted in consideration of a sub-ranges' size of e.g. 0.1 Hz. For each sub-range, a single sine wave is considered, and signal statistic needs to be introduced.

The response function $\mathrm{S(f)}$ is then evaluated based on the transfer function H(f), and the sine sweep amplitude (G(f)), as indicated in Eq. (18).

$$S_i(f_i) = \sqrt{H_i(f_i)} \cdot G_i(f_i) \tag{18}$$

The root mean square (RMS) of a single sine wave can then be evaluated, as indicated in Eq. (19).

$$RMS = \frac{\sqrt{2}}{2} \cdot S_i(f_i) \tag{19}$$

The next step is evaluation of spectral moments for every considered single sine wave function using the following equations for the 0th, 1st, 2nd and 4th spectral moments [Equations (20)–(23)]:

$$m_{0\_sine\_wave}(f_i) = RMS^2 \tag{20}$$

$$m_{1\_sine\_wave}(f_i) = m_0(f_i) \cdot f_i \tag{21}$$

$$m_{2\_sine\_wave}(f_i) = m_0(f_i) \cdot {f_i}^2 \tag{22}$$

$$m_{4\_sine\_wave}(f_i) = m_0(f_i) \cdot {f_i}^4 \tag{23}$$

where $\mathrm{f_i}$ represents the considered frequency.

Signal statistic in frequency domain was based on spectral analysis made iteratively for the considered frequency sub-ranges e.g., 0.1 Hz sub-ranges' width. Spectral moments from deterministic loading ($m_{0\_sine\_wave}$, $m_{1\_sine\_wave}$, $m_{2\_sine\_wave}$, $m_{4\_sine\_wave}$) need to be summed with spectral moments from stochastic background (m_0, m_1, m_2, m_4) as introduced in Equations (24)–(27).

$$m_{0\_mixed\_mode}(f_i) = m_0 + m_{0\_sine\_wave}(f_i) \tag{24}$$

$$m_{1\_mixed\_mode}(f_i) = m_1 + m_{1\_sine\_wave}(f_i) \tag{25}$$

$$m_{2\_mixed\_mode}(f_i) = m_2 + m_{2\_sine\_wave}(f_i) \tag{26}$$

$$m_{4\_mixed\_mode}(f_i) = m_4 + m_{4\_sine\_wave}(f_i) \tag{27}$$

where $m_{0\_mixed\_mode}(f_i)$, $m_{1\_mixed\_mode}(f_i)$, $m_{2\_mixed\_mode}(f_i)$ and $m_{4\_mixed\_mode}(f_i)$ are, respectively, the spectral 0th, 1st, 2nd and 4th moments for superimposed signal at the considered frequency.

It is also required to be noted that during superposition, the spectral moment sum used the full moment from the stochastic part of duty $(\mathrm{m_0}, \mathrm{m_1}, \mathrm{m_2}, \mathrm{m_4})$, as the allowable number of cycles is also calculated iteratively for the considered $\mathrm{T_i}$, which is equal to total time $(\mathrm{T_{Total}})$ divided by the number of sub-ranges; as indicated in Eq. (28),

$$T_i = \frac{T_{\mathrm{Total}}}{n} \tag{28}$$

where n is the number of sub-ranges.

So far as Rainflow Cycle Counting in frequency domain was concerned, the same was evaluated with the use of Dirlik or Narrow Band method, or alternatively damage evaluation was provided for each of the sub-ranges in the same way as introduced in Section 2 of this paper, that is to say by expressing the number of actual cycles according to the Dirlik Rainflow Cycle Counting in frequency domain $(\mathrm{n_i})$; as indicated in Eq. (29),

$$n_i = PDF_i(S) \cdot T_i \cdot E_i[P] \tag{29}$$

where $\mathrm{PDF_i(S)}$ is the PDF at the considered stress bin, and $\mathrm{E_i[P]}$ the number of peaks at the considered stress bin.

The damage value for the considered sub-range $(\mathrm{D_i})$ is as expressed in Eq. (30):

$$D_i = \frac{n_i}{N(S)_i} \tag{30}$$

where $\mathrm{N(S)_i}$ is the allowable number of cycles at the considered stress bin based on the considered S-N curve.

The total damage $(\mathrm{D_{Total}})$ under combined stochastic and deterministic loading is the sum of damage from each of the sub-ranges, as indicated in Eq. (31):

$$D_{Total} = \sum_{i=1}^{n} D_i \tag{31}$$

The damage value obtained by the created algorithm has been benchmarked against the damage value obtained using commercial software, and resultant to this benchmarking, a great correlation was obtained (exemplary results have been introduced in Section 5 of this paper).

4. COMBINED FREQUENCY AND TIME DOMAINS VIBRATION DAMAGE ESTIMATION UNDER COMBINED STOCHASTIC AND DETERMINISTIC LOADING – THE NOVEL METHOD

The new original method developed in the present study assumes the need for processing of the combined frequency and time domain consideration for superimposing the stochastic and

deterministic responses of the considered system. The second stage of the study focussed on developing a novel method for precise vibration damage estimation under combined loading. The idea is based on retrieving time series signal from the frequency domain PSD Response as proposed by Dirlik 5 – with the use of the Monte Carlo method, which is discussed in an extended form in the study of Ptak and Czmochowski 29. The PSD Response function and its corresponding frequency constitute elements of the vector used in retrieval of the time domain signal by employing the inverse discrete Fourier transformation. The equation for time series signal ($S(k\Delta t)$) can be written as follows [Eq. (32)], 5:

$$S(k\Delta t) = \sum_{n=\frac{-N}{2}}^{\frac{N}{2}-1} \theta(j \cdot n2\pi f) \cdot e^{j \cdot 2\pi k_n / N} \tag{32}$$

where f is the considered frequency and N the natural number.
k can be written in the form of the following Eq. (33):

$$k = 0,1,2,3, \ldots, N-1 \tag{33}$$

The θ function can be written in the form of the following Eq. (34), 42:

$$\theta(j \cdot n2\pi f) = \sqrt{S(n \cdot 2\pi\Delta f)}e^{j\Phi_n} \tag{34}$$

for n defined as in Eq. (35).

$$n = 0,1,2,3, \ldots, N/2-1 \tag{35}$$

The Φ_n represents a random phase angle, defined as to be uniformly distributed in the bandwidth <–π; π>. To summarise, the time series is obtained using the Monte Carlo approach and inverse discrete Fourier transformation.

The time series signal can be defined by the function $S(k\Delta t)$ and needs to be a real function of time. This is so as for the introduction of information about stress sign for Rainflow Cycle Counting algorithm, which will be omitted if the complex value of this function is not equal to zero. It implies that the spectrum defined by the function θ in Eq. (34) has to exhibit a complex conjugate symmetry as per the following Eq. (36), 42:

$$\theta(j \cdot n2\pi f) = \theta(-j \cdot n2\pi f) \tag{36}$$

for n defined as in Eq. (35).

A graphical representation of the conjugate symmetry can be found in the figure below (Fig. 6):

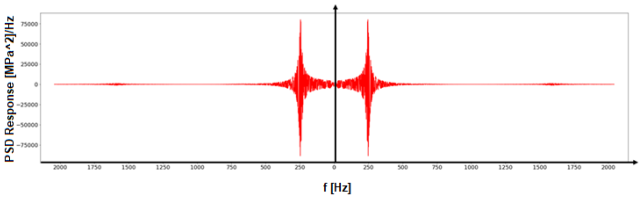

Fig. 6. The complex conjugate symmetry of the PSD Response function

An additional restriction for the θ function is that this function needs to cross zero (37):

$$\theta(0) = 0 \tag{37}$$

Meeting this condition implies that the signal in the time domain S(kΔt) has a mean value equal to zero.

An additional implication is that the imaginary portion of the signal will be equal to zero, and therefore the magnitude of the signal will be equal to the real portion of this signal; and this would moreover imply that the sign can be saved for further fatigue consideration.

For verification of the obtained signal, we evaluated the RMS of the time series signal S(kΔt) using the standard deviation equation, which can be written as shown below in Eq. (38):

$$\mathrm{RMS}_{\text{time series}} = \sqrt{\frac{1}{N}\sum_{k=0}^{N-1} S(k\Delta t)^2} \tag{38}$$

The time signal has a zero-mean value, and the standard deviation equal to RMS was estimated for a signal in the frequency domain. Therefore, retrieval of a signal defined in the frequency domain to one in the time domain has been carried out successfully, and this methodology will be used for retrieving the fatigue information by employing time series Rainflow Cycle Counting algorithm, which is implemented in the Python language (as documented 44).

For evaluating the damage in the time domain, the authors of the Rainflow Cycle Counting algorithm have used a Python language program 46, which allows the fatigue cycles to be counted and appropriate range values for time series signal (peak and trough extraction from time series signals) to be ascertained.

Time series signals retrieved from the PSD Response signal with the use of the developed Python algorithms are indicated in Fig. 7 (frequency resolution based on N = 216). Additionally, the Rainflow Cycle Counting histogram for this signal has been introduced in Fig. 8.

Note: In the present research, the stress life method has been introduced as an example. Further research will focus on using the strain life method, and would involve the use of e.g. Morrow or Smith–Watson–Topper mean stress correction and Neuber correction [48–50].

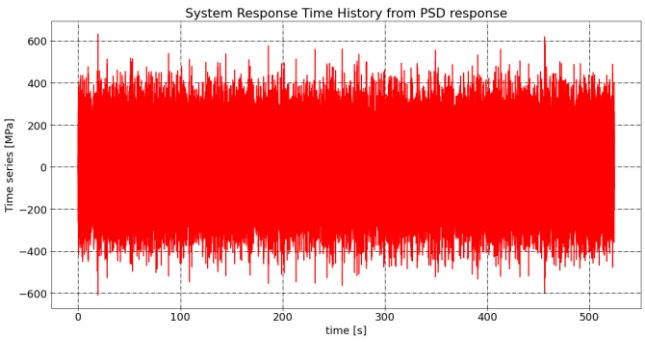

Fig. 7. Initial time series processing extracting peak and trough for Rainflow Counting algorithm, white noise signal, irregular factor 0.3, block size N = 2^{16}

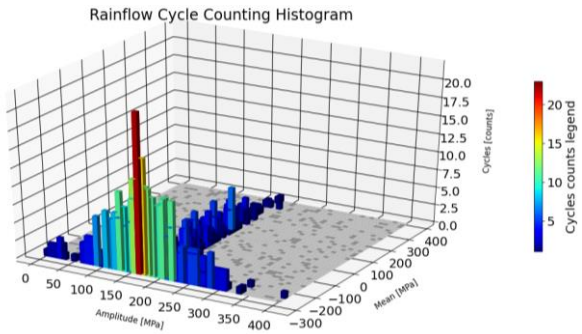

Fig. 8. Rainflow Cycle Counting algorithm histogram, white noise signal, irregular factor 0.3, block size N = 2^{16}

The specified linear sine sweep frequency ($f_{spec}(t)$) dependence from time can be written as a function of time and frequency, as indicated in Eq. (39):

$$f_{spec}(t) = f_1 + K \cdot T \tag{39}$$

where T is the total sweep time, K the sweep rate and f_1 the initial sweep frequency.

Specified frequency ($f_{spec}(t)$) can be written in an alternative form, as indicated in Eq. (40):

$$f_{spec}(t) = f_1 + (f_2 - f_1)\frac{t}{T} \tag{40}$$

where f_2 is the end sweep frequency and t the time variable.

Sine sweep frequency ($f(t)$) is the integral of specified frequency and can be written as indicated in Eq. (41):

$$f(t) = \int f_{spec}(t)dt = f_1 \cdot t + \frac{f_2 - f_1}{T} \cdot \frac{t^2}{2} \tag{41}$$

Input sine sweep ($G(t)$) with constant accelaration amplitude can be written as indicated in Eq. (42):

$$G(t) = u(t) \cdot \sin(\omega t) = u(t) \cdot \sin(2\pi f(t) \cdot t) \tag{42}$$

where $u(t)$ is the displacement in time and ω the circular frequency.

Additionally, the equivalent version for implementation in the Python programming language 44 can be written as indicated in Eq. (43):

$$G(t) = u(t) \cdot \sin\left(2\pi \cdot t \cdot \left(f_1 + \frac{f_2 - f_1}{T} \cdot \frac{t}{2}\right)\right) \tag{43}$$

As the sine sweep frequency is deterministic, that is to say since it depends on time, the same can thus be scaled by the transfer function H(f) to obtain a time series sweep including the system response, as indicated in Fig. 9.

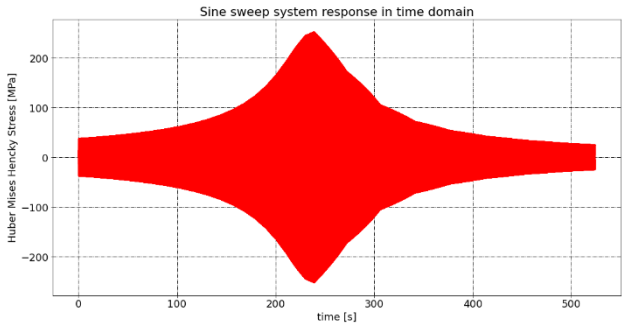

Fig. 9. Sine sweep system response in the time domain, sweep rate K = 0.095367 Hz/s

Sine sweep response ($S(t)$) can be written as indicated in Eq. (41):

$$S(t) = \sqrt{H(t)} \cdot G(t) \tag{44}$$

where H(f) is the transfer function and G(t) the input sine sweep acceleration.

This signal, which consists of the PSD Response stress values, can now be superimposed to the random time series PSD Response retrieved using the Monte Carlo method (assuming system linearity, with a restriction pertaining to the time sequence of the retrieved random signal needing to match with the time sequence of the sine sweep) – as can be seen from Fig. 10.

For the superimposed signal corresponding to the Rainflow Cycle Counting algorithm in the time domain to be capable of being used, the S–N curve for the stress life method needs to be introduced, and it is only then that the damage for the combined stochastic–deterministic input can be evaluated.

It also needs to be noticed that sweep rate can be fitted to background random loading to obtain one sweep during acting random loading if there is no specific requirement specified by the aircraft manufacturer.

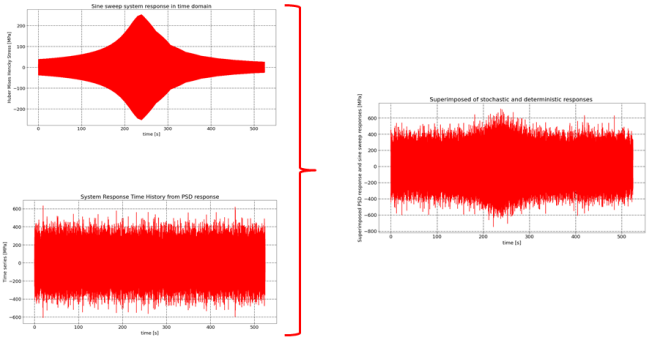

Fig. 10. Superimposition of stochastic and deterministic responses in the time domain

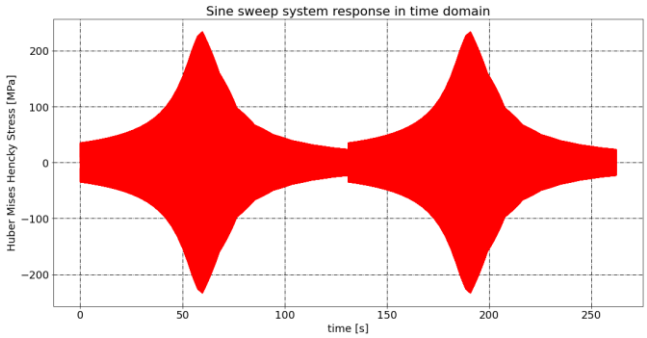

Fig. 11. Sine sweep system response in the time domain, sweep rate K·2 = 0.190735 Hz/s

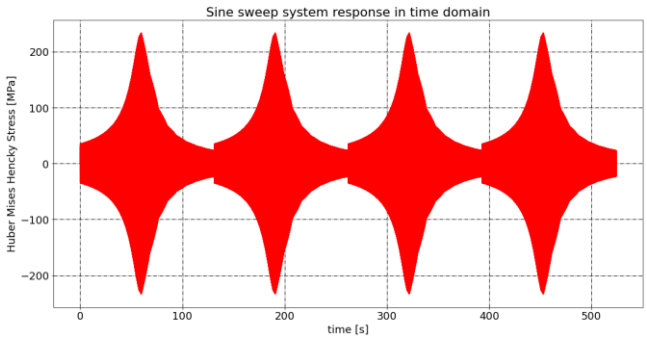

Fig. 12. Sine sweep system response in the time domain, sweep rate K·4 = 0.38147 Hz/s

It has been ascertained that n number of sine sweeps with n times higher than the reference sweep rate (Fig. 11 for n = 2 and Fig. 12 for n = 4) cause the same theoretical damage as one sweep with the reference sweep rate. For benchmark signals have been merged in a theoretical way, there is no continuous link between sweeps; however, the impact on the quoted damage is negligible as the maximum stress cycles for the considered sam-

ples are much higher than those in the link region. It needs to be noticed that only one sweep acting during random loading duration should give the highest damage as increasing the sweep rate can cause a situation wherein the system will not respond with full amplitude during the resonance and the maximum resonance amplitude will decrease.

A proposed algorithm flow chart for damage estimation under combined stochastic and deterministic loading in the time domain is presented in Fig. 13.

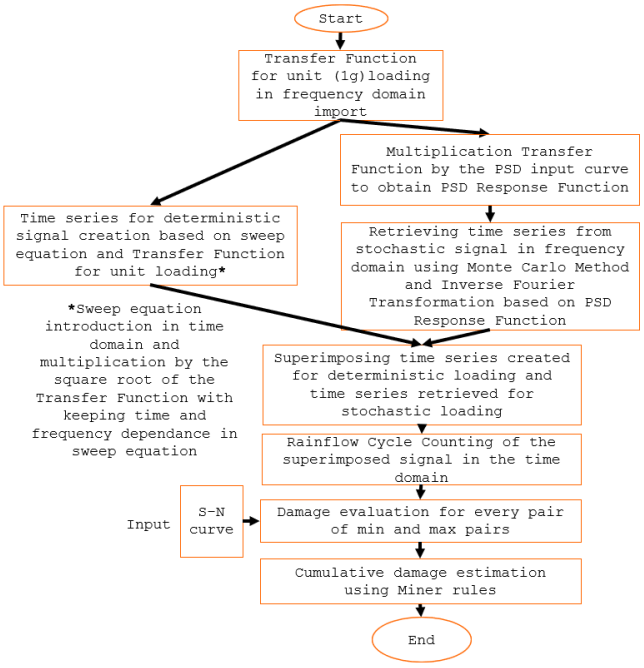

Fig. 13. Algorithm flow chart for damage estimation under combined stochastic and deterministic loading in the time domain

5. COMPARISON RESULTS OBTAINED FOR LEGACY METHOD AND PROPOSED METHOD

The abovementioned legacy method for combined stochastic–deterministic loading proved to be highly conservative. Two loops of analysis under vibration loading were calculated. The 1st loop, based on algorithms for vibration damage estimation under deterministic loading (pure sine sweep), obtained a damage value of 0.009 for the critical integration point. The 2nd loop was based on algorithms for combined stochastic–deterministic loading and a low-level non-damaging random load (giving rise to a damage of 0 after evaluation using the algorithm for pure random loading and peaking at 9 MPa in the case of a stress of 5 σ). For the combined load scenario, a damage of 0.58 was calculated for the same sine sweep as in the 1st loop (resulting in a damage of 0.009). The results above have shown that the legacy approach is characterised by a high conservatism and have initialised the subsequent phase of our research. A summary of the obtained result is provided in Tab. 2.

Note: Even when assuming that maximum stress from resonance for sine sweep (258 MPa) occurs for every cycle in sweep (conservatively assuming that the maximum peak in a resonance occurs through 50 Hz) and superimposing a 5 σ stress amplitude equal to 9 MPa, the damage obtained is equal to 0.21.

The research results show that the legacy method is highly conservative, and therefore the need arises for developing a new method for this loading scenario, to remove the conservatism during damage estimation. This is important from the point of view of requirements associated with aerospace, especially for military application, where e.g., the mass of the components can be reduced.

Tab. 2. Comparison damage evaluated with spectral method in the frequency domain (legacy method) and new proposed method (damage evaluated in the time domain)

Test No.	1	2
Damage proposed method	0.00875	0.06718
Damage legacy method authors algorithm for combined loading	0.58110	1.00792
Damage legacy method MSC CAE Fatigue algorithm for combined loading	0.60804	1.07479
Damage for sine sweep only using authors algorithm for deterministic harmonic loading	0.00875	0.00875
Damage for sine sweep only using authors algorithm for deterministic harmonic loading	0.00944	0.00944

6. ADDITIONAL RESULTS DERIVED FROM RESEARCH ON PROPOSED METHOD

Results derived from research on the pure stochastic loading scenario show that damage varies, and the variation depends on the block size (N) used in the inverse Fourier transformation. Since there was a need for obtaining information about the statistic of the damage as well as for deriving the damage distribution, the research has been extended to a large search population consisting of 5,000 samples.

The research was performed for white noise signal. Wide and narrow band signals will be introduced in further research. Additionally introduced were three different block sizes: 212, 214 and 216. For fitting distribution, we used the Kolmogorov–Smirnov criterion, which assesses the probability of distribution. For testing, we used the different distribution types available in the Python library 44. The best-fitted distributions have been narrowed down to three with the highest probability of fitting: Gaussian, Exponentiated Weibull and Generalized Extreme Value distributions.

Note that variation of damage for the considered distribution is low as per Tabs. 3–8.

In Fig. 14, Fig. 16 and Fig. 18, corresponding damage values were presented for the searched population for white noise signal for three mentioned block sizes for signal clipped at 3 standard deviation. Proceeding based on analogy, the same results for signal clipped at 5 standard deviation have been presented in Fig. 20, Fig. 22 and Fig. 24.

The best-fitted distributions' visualisations for signal clipped at 3 standard deviation for three block sizes have been presented in Fig. 15, Fig. 17 and Fig. 19. Proceeding based on analogy, the results for signal clipped at 5 standard deviation have been presented in Fig. 21, Fig. 23 and Fig. 25.

In Tab. 3–Tab. 5, we introduced a populational research results' summary made for white noise signal clipped at 3 standard deviation and in Tab. 6–Tab. 8 a summary of results for signal clipped at 5 standard deviation.

DOI 10.2478/ama-2023-0065

acta mechanica et automatica, vol.17 no.4 (2023)
Special Issue "Computational Technologies in Engineering TKI2022

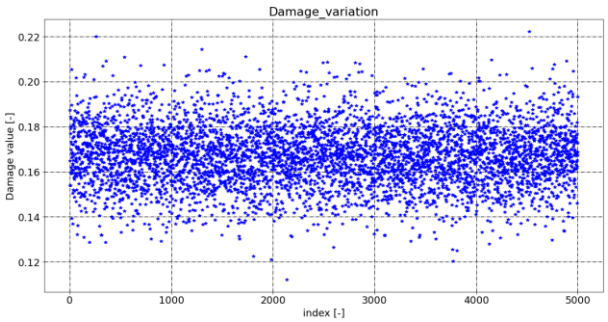

Fig. 14. Damage values for searched population for white noise signal, signal clipped at 3 standard deviations, block size N = 2^{12}

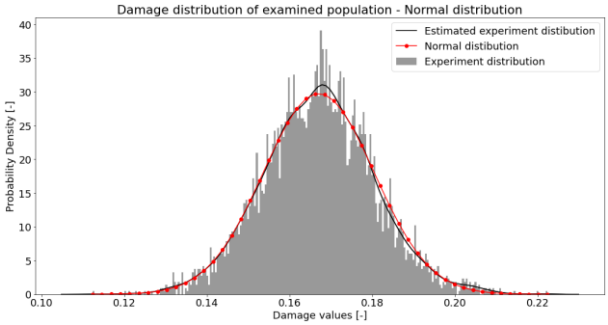

Fig. 15. Best-fitted distribution for damage values for searched population for white noise signal, signal clipped at 3 standard deviations, block size N = 2^{12} – Normal distribution

Tab. 3. Statistical parameters for white noise signal clipped at 3 standard deviations, block size N = 2^{12}

Distribution type	Normal	Exponentiated Weibull	Generalized Extreme Value
Probability of fitted distribution [-]	0.27452	0.00000	0.00091
Mean damage [-]	0.16697	0.15973	0.16708
Standard deviation of damage [-]	0.01341	0.04217	0.01380
0.13% not lower than quoted value of damage [-]	0.12660	0.11231	0.13093
99.73% not exceed quoted value of damage [-]	0.20427	0.33518	0.20641

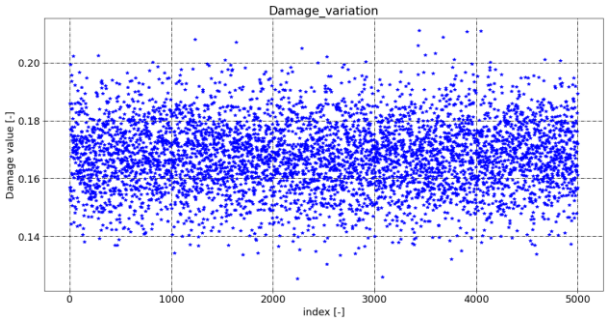

Fig. 16. Damage values for searched population for white noise signal, signal clipped at 3 standard deviations, block size N = 2^{14}

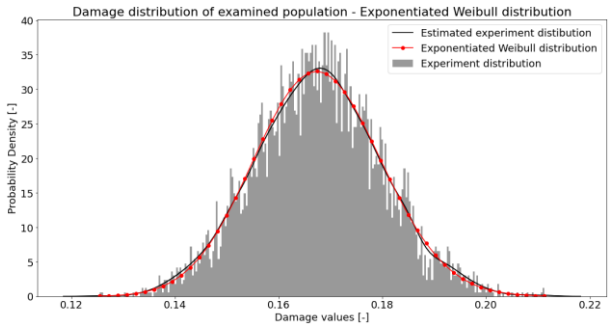

Fig. 17. Best-fitted distribution for damage values for searched population for white noise signal, signal clipped at 3 standard deviations, block size N = 2^{14} – Exponentiated Weibull distribution

Tab 4. Statistical parameters for white noise signal clipped at 3 standard deviations N = 2^{14}

Distribution type	Normal	Exponentiated Weibull	Generalized Extreme Value
Probability of fitted distribution [-]	0.80900	0.90471	0.05506
Mean damage [-]	0.16763	0.16763	0.16768
Standard deviation of damage [-]	0.01217	0.01217	0.01235
0.13% not lower than quoted value of damage [-]	0.13098	0.13269	0.13450
99.73% not exceed quoted value of damage [-]	0.20149	0.20201	0.20164

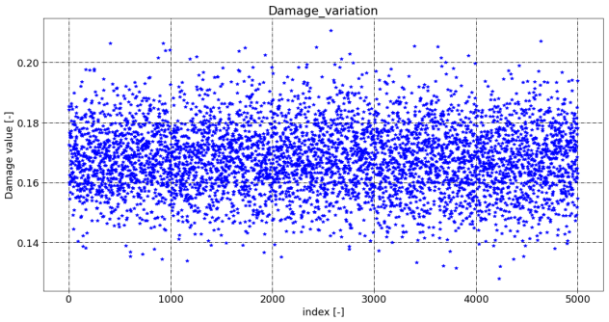

Fig. 18. Damage values for searched population for white noise signal, signal clipped at 3 standard deviations, block size N = 2^{16}

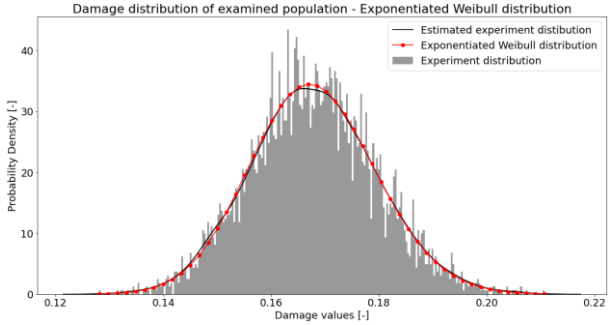

Fig. 19. Best-fitted distribution for damage values for searched population for white noise signal, signal clipped at 3 standard deviations, block size N = 2^{16} – Exponentiated Weibull distribution

Tab. 5. Statistical parameters for white noise signal clipped at 3 standard deviations N = 2^{16}

Distribution type	Normal	Exponentiated Weibull	Generalized Extreme Value
Probability of fitted distribution [-]	0.49042	0.99708	0.26514
Mean damage [-]	0.16785	0.16783	0.16789
Standard deviation of damage [-]	0.01161	0.01162	0.01175
0.13% not lower than quoted value of damage [-]	0.13287	0.13473	0.13660
99.73% not exceed quoted value of damage [-]	0.20016	0.20152	0.20064

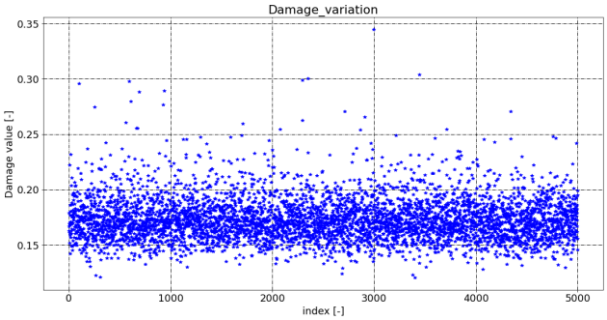

Fig. 20. Damage values for searched population for white noise signal, signal clipped at 5 standard deviations, block size N = 2^{12}

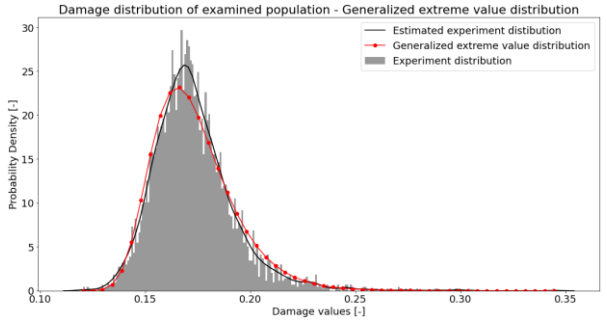

Fig. 21. Best-fitted distribution for damage values for searched population for white noise signal, signal clipped at 5 standards deviations, block size N = 2^{12} – Generalized Extreme Value distribution

Tab. 6. Statistical parameters for white noise signal clipped at 5 standard deviations, block size N = 2^{12}

Distribution type	Normal	Exponentiated Weibull	Generalized Extreme Value
Probability of fitted distribution [-]	0.00000	0.00001	0.00049
Mean damage [-]	0.17292	0.17277	0.17313
Standard deviation of damage [-]	0.01933	0.01827	0.01932
0.13% not lower than quoted value of damage [-]	0.11472	0.12702	0.13327
99.73% not exceed quoted value of damage [-]	0.22669	0.23245	0.24754

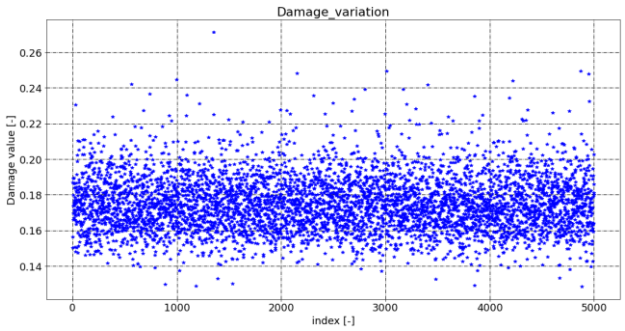

Fig. 22. Damage values for searched population for white noise signal, signal clipped at 5 standard deviations, block size N = 2^{14}

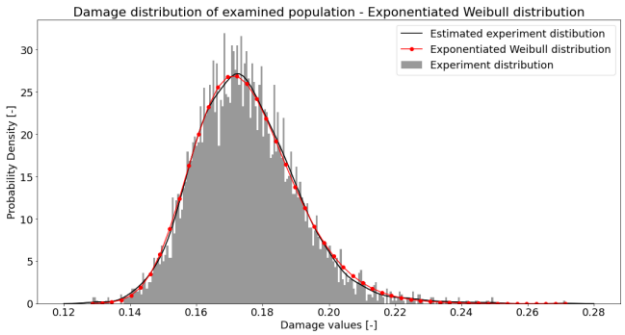

Fig. 23. Best-fitted distribution for damage values for searched population for white noise signal, signal clipped at 5 standard deviations, block size N = 2^{14} – Exponentiated Weibull distribution

Tab. 7. Statistical parameters for white noise signal clipped at 5 standard deviations, block size N = 2^{14}

Distribution type	Normal	Exponentiated Weibull	Generalized Extreme Value
Probability of fitted distribution [-]	0.00000	0.68282	0.07246
Mean damage [-]	0.17498	0.17495	0.17512
Standard deviation of damage [-]	0.01547	0.01541	0.01576
0.13% not lower than quoted value of damage [-]	0.12840	0.13748	0.13901
99.73% not exceed quoted value of damage [-]	0.21801	0.22694	0.22855

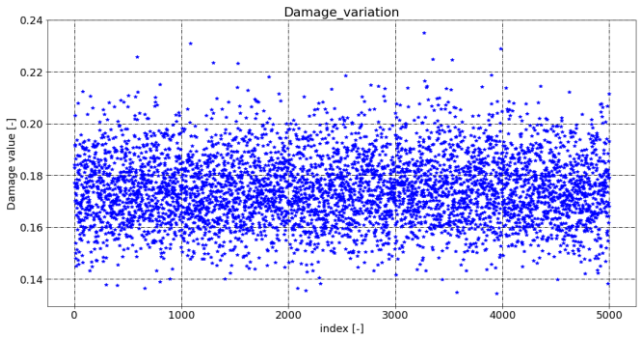

Fig. 24. Damage values for searched population for white noise signal, signal clipped at 5 standard deviations, block size N = 2^{16}

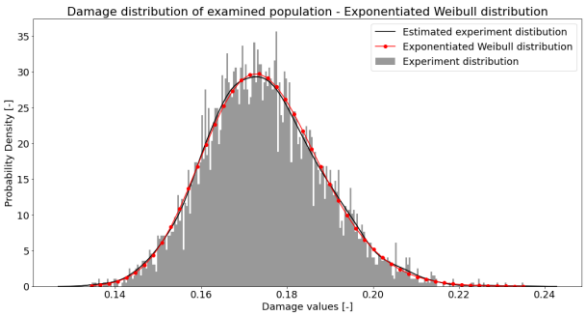

Fig. 25. Best-fitted distribution for damage values for searched population for white noise signal, signal clipped at 3 standard deviations, block size N = 2^{16} – Exponentiated Weibull distribution

Tab. 8. Statistical parameters for white noise signal clipped at 5 standard deviations, block size N = 2^{16}

Distribution type	Normal	Exponentiated Weibull	Generalized Extreme Value
Probability of fitted distribution [-]	0.00193	0.83692	0.52516
Mean Damage [-]	0.17462	0.17463	0.17467
Standard Deviation of Damage [-]	0.01354	0.01354	0.01370
0.13% not lower than quoted value [-]	0.13384	0.13902	0.14047
99.73% not exceed quoted value [-]	0.21230	0.21650	0.21627

The conclusion, based on the aforementioned research results, is that every three distributions selected as final give similar mean value and standard deviation for the considered signal, which match to the experimental mean value and standard deviation. Additionally quoted is the value of damage involved in assessing the damage variation. For this purpose, the quoted value of damage for which 99.73% of the population have a lower value of damage is: mean, +3 standard deviation in normal distribution; and the damage value for which 0.13% of the population have a lower value of damage is: mean, –3 standard deviation. The first damage value quoted will be needed for sizing units for the considered load scenario. The second damage quoted can be used to avoid undertesting during real testing. For example, for damage quoted in Tab. 8, testing should be carried out for the increased duty to obtain a mean –3 standard deviation that is higher than or equal to the +3 standard deviation obtained for the original duty (mean –3 standard deviation damage needs to be increased from 0.13902 for original duty to a minimum of 0.21650 for increased duty) – this approach would ensure that unit will not be undertested during real testing.

Research results show that the Exponentiated Weibull distribution is the best fitted, when the block size is adequately large – i.e., Nx ≥N = 214. (Some anomalies were observed in Weibull distribution for smaller values, as shown in Tab. 3, and additionally damage variation is higher than for larger block size.) Therefore, for the final choice, we may decide to use the Exponentiated Weibull distribution to arrive at a statistical description of damage values for the considered population.

Additionally, research results show that for stochastic and deterministic combination loading scenario, the variability of damage is closed for different block sizes used, in opposition to the situation prevailing concerning the only random load scenario (3 standard variation is around +/–20% for N = 212, N = 214 and N = 216, as shown in Tab. 3–Tab. 5 andTab. 6–Tab. 8). For the only random loading scenario, damage variability for block size N = 212 can be around +/–60%; however, for block size N = 216, the same can be around 13% and for block size N = 220 it can be around 2%. Therefore, for combined stochastic and deterministic loading, N = 214 is recommended, as for this block size we observed stabilisation of damage variation and obtained a calculation accuracy close to those associated with higher block sizes. This value of block size implies the best relational performance with regard to accuracy.

7. SUMMARY AND CONCLUSION

A summary of the computer experiments conducted with the use of the two combined methods is provided in this section. FEM, Monte Carlo method and Python programming allow identification of the high conservativism of the legacy frequency domain-based method. The research results presented in this paper show that the legacy method used by commercial software for combined stochastic–deterministic loading scenarios gives highly conservative damage results, which might result in oversizing military aircraft or helicopters units.

The introduction of a novel method of calculation (based on combined frequency and time approach) of damage under the mentioned loading scenario allows us to precisely perform damage estimation in the time domain together with maintaining the efficiency benefit related to frequency domain calculation. Using the novel method introduced in this paper allows us to obtain a higher accuracy of the results than the legacy method, as well as an efficiency of computation that, in comparison with the legacy method, is at least comparable if not higher.

The research result reveals that damage variation is constant (characterised by a small variability depending on the block size used in the inverse Fourier transformation, in opposition to the only random loading scenario as quoted in related research 29). Therefore, the conclusion of the presented research is that for high amplitude sweep having a simultaneous random nature, it is recommended to use N = 214 as the block size.

This novel method allows also for analysis of time series population to assess the damage variation, which is impossible with use of the legacy method. An additional conclusion is that for populational analysis, it is recommended to use Exponentiated Weibull distribution for statistical consideration.

An additional benefit related to using the proposed method is that the signal can be clipped with a requested standard deviation level e.g., in aerospace industry, it is common to clip the input to 3 standard deviations. Therefore, this method can replicate real test conditions, which is not possible with the use of the spectral method.

Another aspect is that an algorithm can be also fitted to align with frequency resolution (block size) during conduction of real tests to assess what the variability of damage will be for test rig equipment. As for block sizes smaller than N = 214, the variability might increase, which can imply undertesting.

Further research results will focus on research on wide band and narrow band signals. Additional aspects are an implementation strain life method for highly loaded parts and the development of software for aerospace application with the use of the research

results presented in this paper.

Additionally, the Critical Plane approach will be introduced for defining PSD Response function. Future research will also be expanded to ascertain whether it is possible to synergistically use energy fracture mechanics methods, e.g., Cohesive Zone Model method, for damage estimation and life prediction.

REFERENCES

1. Bendat J. Probability functions for random responses. NASA report contract NAS-5-4590, 1964. Available from: https://ntrs.nasa.gov/citations/19640008076
2. Bendat J. Random data: Analysis and measurement procedures. John Wiley & Sons Inc., New York United States 2010
3. Bendat J. Principles and Applications of Random Noise Theory. John Wiley, New York,1958
4. Rice S. Mathematical analysis of random noise. Selected papers on noise and stochastic processes, Dover, New York, 1954
5. Dirlik T. Application of computers to fatigue analysis, PhD Thesis, Warwick University, 1985. Available from: http://wrap.warwick.ac.uk/2949/
6. CAEfatigue VIBRATION (CFV) User Guide & Verification Manual (Release 2020). CAEfatigue Limited, UK, Nov 2020.
7. nCode 2022.0 documentation, HBK 2022.
8. Lalanne C. Mechanical vibration and shock, Vol. 4, Hermes Penton Science, London, 2009
9. Lalanne C. Mechanical vibration and shock analysis: Specification Development, 3rd edition, Vol. 5, Wiley, London, 2014
10. Lalanne C. Mechanical vibration and shock analysis: Fatigue Damage, 3rd edition, Vol. 4, Wiley, London, 2014
11. Steinberg D. Vibration analysis for electronic equipment (2nd edition). Jon Wiley & Sons, New York, 1988
12. Halfpenny A, Kichim F. Rainflow cycle counting and acoustic fatigue analysis technique for random loading. 10th International Conference RASD, Southampton UK, 2010. Available from:
13. http://www.vibrationdata.com/tutorials2/Paper_RASD2010_005_Halfpenny_Kihm.pdf
14. Halfpenny A. Rainflow Cycle Counting and Fatigue Analysis from PSD, Proceedings of the ASTELAB conference, France, 2007. Available from: https://core.ac.uk/download/pdf/42735102.pdf
15. Halfpenny A, Bishop N. Vibration Fatigue, HBM-nCode, UK, 1997
16. Sweitzer K., Bishop N, Genberg V. Efficient computation of spectral moments for determination of random response statistics. International Conference on Noise and Vibration Engineering - ISMA, Leuven, BE, 2004. Available from:https://citeseerx.ist.psu.edu/docment?repid=rep1&type=pdf&doi=dd17f690eeac37cf88649cdf823507ca0ffd1f1c
17. Bishop N, Sherratt F. Finite Element Based Fatigue Calculation. NAFEMS Ltd., 2000, https://doi.org/10.59972/ta5h05jd
18. Bishop N. Methods for the rapid evaluation of fatigue damage on the Howden HWP330 wind turbine. Proceedings of 13th British Wind Energy Conference, Swansea, UK, p. 317-321, 1991
19. Bishop N, Sweitzer K, Schlesinger D, Woodward A. Fatigue calculation for multi input random and deterministic loads in the frequency domain. UK NAFEMS Conference, Oxford IK, Accelerating the Future of CAE, 10-11 June 2014.
20. Bishop N, Kerr S, Murthy P, Sweitzer K. Advances Relating to Fatigue Calculations for Combined Random and Deterministic Loads. SAE Technical Paper 2014-01-0725, 2014 https://doi.org/10.4271/2014-01-0725
21. Bishop N, Murthy P, Sweitzer K. Advances Relating to Fatigue Calculation for Combined Random and Deterministic Loads. 13th International ASTM/ESIS Symposium on Fatigue and Fracture Mechanics (39th National Symposium on Fatigue and Fracture Mechanics), November 13-15, 2013, Jacksonville, FL https://doi.org/10.4271/2014-01-0725
22. Bishop N, Murthy P, Sweitzer K., Kerr S. Time vs frequency domain analysis for large automotive systems. SAE Technical Paper 2015-01-0535, 2015. https://doi.org/10.4271/2015-01-0535
23. Bishop N, Murthy P, Sweitzer K., Kerr S. Time vs frequency domain analysis for large automotive systems. SAE Technical Paper 2015-01-0535, 2015, doi: https://doi.org/10.4271/2015-01-0535
24. Ferreira W, Meehan T, Cardoso V, Bishop N. A comparative study of automotive system fatigue models processed in the time and frequency domain. SAE Technical Paper 2016-01-0377, 2016, https://doi.org/10.4271/2016-01-0377
25. Datta S, Bishop N, Sweitzer K, Atkins A. Simultaneous durability assessment and relative random analysis under base shake loading conditions. SAE Technical Paper 2017-01-0339, 2017
26. https://doi.org/10.4271/2017-01-0339
27. MIL-STD-810H, Department of Defence Test Method Standard: Environmental Engineering Consideration and Laboratory Test, USA, 2019.
28. Brown AM, McGhee DS. Statistical Evaluation and Improvement of Method for Combining Random and Harmonic Loads. Marshall Space Flight Centre, Alabama 35812, 2003. Available from: https://ntrs.nasa.gov/citations/20030017832
29. Ptak M, Czmochowski J. Using computer techniques for vibration damage estimation under stochastic loading using the Monte Carlo Method for aerospace applications. Probabilistic Engineering Mechanics. 2023, vol. 72, p. 1-13. https://doi.org/10.1016/j.probengmech.2023.103452
30. Ptak M, Czmochowski J. Using computer techniques for vibration damage estimation of aircraft structures under stochastic loading. W: Computer Aided Engineering. Nauka i przemysł / red. Tadeusz Smolnicki. Wrocław : Oficyna Wydawnicza Politechniki Wrocławskiej, 2022. p. 169-179. ISBN: 978-83-7493-223-3
31. Metallic Materials Properties Development and Standardization (MMPDS-15), Battelle Memorial Institute, July 2020.
32. Delprete C, Sesana R, Vercelli A. Multiaxial damage assessment and life estimation: application to an automotive exhaust manifold. Procedia Engineering Vol. 2, April 2010, p. 725-734. Available from: doi: 10.1016/j.proeng.2010.03.078
33. Engin Z., Coker D. Comparison of Equivalent Stress Method with Critical Plane Approaches for Multiaxial High Cycle Fatigue Assessment. 2nd International Conference on Structural Integrity, ICSI 2017, 4-7 September 2017, Funchal, Madeira, Portugal. Procedia Structural Integrity Vol. 5 2017, p. 1229-1236. Available from: doi: 10.1016/j.prostr.2017.07.049
34. Smolnicki M, Ptak M, Lesiuk G. Static failure load predictions in notched steel components using a combined experimental-numerical approach. International Journal of Structural Integrity. 2017, vol. 8, no. 6, p. 683-693.https://doi.org/10.1108/IJSI-05-2017-0032
35. Wang JT. Relating Cohesive Zone Models to Linear Elastic Fracture Mechanics. NASA/TM-2010-216692, May 2010. Available from: https://ntrs.nasa.gov/api/citations/20100021117/downloads/20100021117.pdf
36. Kucharski P, Lesiuk G, Czapliński T, Fratczak R, Maciejewski Ł. Numerical Estimation of Stress Intensity Factors and Crack Propagation in Lug Connector with Existing Flaw. AIP Conference Proceedings. Fatigue Failure and Fracture Mechanics XXVI: Proceedings of the XXVI Polish National Conference on Fatigue Failure and Fracture Mechanics 17-20 May 2016 Fojutowo, Poland. https://doi.org/10.1063/1.4965949
37. Miner A. Cumulative damage in fatigue. J Applied Mechanics, Vol. 67, 1945, pp A159-A164, 1945.
38. Palmgren A. Die lebensdauer von kugellagern, zeitschrift des vereinesdeutscher ingenierure, Vol. 68, No. 14, 1924, pp. 339-341, 1924
39. Zienkiewicz O.C. Finite Element Method. McGraw-Hill, Dallas (1977)
40. ABAQUS User Manual V2018. Dassault Systems (2017)
41. Ptak M, Czmochowski J. Analysis of the impact of dynamic loads on transmission shafts of a civil aircraft. Modelling in engineering 2020: applied mechanics, Springer 2021. p. 245-257. Available from: doi: 10.1007/978-3-030-68455-6_22

42. Newland D. An introduction to random vibrations, spectral & wavelet analysis. Longman Inc., England 1995
43. Langtangen H. Python Scripting for Computational Science, Third Edition, Simula Research Laboratory. Springer, Berlin, Heidelberg, 2009
44. Python 3.8.12 Documentation (https://docs.python.org/3.8/)
45. Python 2.7.3 Documentation (https://docs.python.org/release/2.7.3/)
46. ESDU 06010 Cycle counting methods for the estimation on fatigue life
47. Matsuishi M, Endo T. Fatigue of metals subject to varying stress. Japan Society of Mechanical Engineers, Fukuoka, March 1968
48. Downing S, Socie D. Simple Rainflow counting algorithms. International Journal of Fatigue, January 1982
49. Watson P, Dabell B. Cycle counting and fatigue damage. Society of Environmental Engineers, September 1976
50. Dowling NE.. Local Strain Approach to Fatigue. Comprehensive Structural Integrity, Vol 4, 2003 p. 77-94. Available from: https://www.researchgate.net/publication/309717379_Comprehensive_Structural_Integrity
51. Meggiolaro MA, Castro JTP. Statistical evaluation of strain-life fatigue crack initiation predictions. International Journal of Fatigue, Vol 26, Issue 5, May 2004, p. 463-476. Available from: doi:10.1016/j.ijfatigue.2003.10.003
52. Lee YL, Hathaway R, Barkey M. Fatigue Testing and Analysis. Theory and Practice. Elsevier Butterworth Heinemann, 1st Edition July 29, 2004.

Michal Ptak: https://orcid.org/0000-0001-7308-8881
Jerzy Czmochowski: https://orcid.org/0000-0001-9547-7802